

Neuronal-type-specific epigenome editing to decrease *SNCA* expression: Implications for precision medicine in synucleinopathies

Zhiguo Sun,¹ Boris Kantor,² and Ornit Chiba-Falek^{3,4}

¹CLAIRigene, LLC, Durham, NC 27701, USA; ²Viral Vector Core, Department of Neurobiology, Duke University School of Medicine, Durham, NC 27710, USA; ³Division of Translational Brain Sciences, Department of Neurology, Duke University School of Medicine, Durham, NC 27710, USA; ⁴Center for Genomic and Computational Biology, Duke University School of Medicine, Durham, NC 27710, USA

Overexpression of *SNCA* has been implicated in the pathogenesis of synucleinopathies, particularly Parkinson's disease (PD) and dementia with Lewy bodies (DLB). While PD and DLB share some clinical and pathological similarities, each disease presents distinct characteristics, including the primary affected brain region and neuronal type. We aimed to develop neuronal-type-specific *SNCA*-targeted epigenome therapies for synucleinopathies. The system is based on an all-in-one lentiviral vector comprised of CRISPR-dSaCas9 and guide RNA (gRNA) targeted at *SNCA* intron 1 fused with a synthetic repressor molecule of Krüppel-associated box (KRAB)/ methyl CpG binding protein 2 (MeCp2) transcription repression domain (TRD). To achieve neuronal-type specificity for dopaminergic and cholinergic neurons, the system was driven by tyrosine hydroxylase (TH) and choline acetyltransferase (ChAT) promoters, respectively. Delivering the system into human induced pluripotent stem cell (hiPSC)-derived dopaminergic and cholinergic neurons from a patient with the *SNCA* triplication resulted in efficient and neuronal-type-specific downregulation of *SNCA*-mRNA and protein. Furthermore, the reduction in *SNCA* levels by the gRNA-dSaCas9-repressor system rescued disease-related cellular phenotypes including Ser129-phosphorylated α -synuclein, neuronal viability, and mitochondrial dysfunction. We established a novel neuronal-type-specific *SNCA*-targeted epigenome therapy and provided *in vitro* proof of concept using human-based disease models. Our results support the therapeutic potential of our system for PD and DLB and provide the foundation for further pre-clinical studies in animal models toward investigational new drug (IND) enablement and clinical trials.

INTRODUCTION

Synucleinopathies are neurodegenerative disorders that share a common pathological lesion of intracellular protein aggregates largely composed of the α -synuclein protein,^{1–5} known as Lewy bodies (LBs) and Lewy-related neurites. While these spectrum diseases exhibit neuropathological similarities, each disease presents distinct characteristics. For example, the cell types and brain regions containing the LBs differ, particularly in early disease stages, so that, while

LBs in dopaminergic neurons are the primary early disease characteristic of Parkinson's disease (PD),^{6–8} early stages of dementia with Lewy bodies (DLB) has LBs primarily in the amygdala and cerebral cortex, as well as basal forebrain cholinergic neurons.^{9–12}

Genetic studies including genome-wide association studies (GWASs) for the most common synucleinopathies, PD and DLB, have implicated *SNCA* gene, which encodes the α -synuclein protein, as a highly significant genetic risk factor for these diseases.^{13–24} Although the precise mechanisms underlying the associations of *SNCA* with PD and DLB are yet to be discovered, accumulating evidence suggests that overexpression of *SNCA* may play a crucial role in etiology of these diseases (reviewed in Tagliaferro and Chiba-Falek²⁵). Notably, elevated levels of *SNCA* were described in disease-affected brain tissues compared to healthy controls.^{26–30} Moreover, lowering *SNCA* levels has demonstrated a beneficial impact.^{31–33} Changes in the levels of *SNCA* expression are regulated by different factors, including epigenetics.³⁴ Specifically, the role of DNA methylation across *SNCA* intron 1 was studied in relation to *SNCA* dysregulation in the context of disease.^{35–38} Thus, epigenetic editing is an attractive approach for manipulation of *SNCA* expression back to normal physiological levels.

Previously, we developed a novel epigenome-editing approach that utilizes an all-in-one lentiviral vector (LV) harboring deactivated (d)Cas9-DNA methyltransferase 3A (DNMT3A) to modulate expression of *SNCA* gene mediated by modification of DNA-methylation within a CpG island at the *SNCA* intron 1 region.^{39,40} We showed that the system resulted in a precise and moderate downregulation (30%) of *SNCA* overexpression in human induced pluripotent stem cell (hiPSC)-derived ventral midbrain (MD) progenitor neurons

Received 7 March 2023; accepted 22 November 2023;
<https://doi.org/10.1016/j.omtn.2023.102084>.

Correspondence: Boris Kantor, Viral Vector Core, Department of Neurobiology, Duke University School of Medicine, Durham, NC 27710, USA.

E-mail: boris.kantor@duke.edu

Correspondence: Ornit Chiba-Falek, Division of Translational Brain Sciences, Department of Neurology, Duke University School of Medicine, Durham, NC 27710, USA.

E-mail: o.chibafalek@duke.edu



from a PD patient with the triplication of the *SNCA* locus (SNCA-Tri).^{39,40} Notably, the reduction of *SNCA* expression mediated by the developed technology was sufficient to ameliorate phenotypic perturbations characteristic of the SNCA-Tri cells, including rescuing the vulnerability to increased production of mitochondrial superoxide and the cellular viability.³⁹ In this study, we aimed to refine the system such that it would target specifically dopaminergic and cholinergic neurons that are afflicted in PD and DLB, respectively. We modified the all-in-one LV dCas9-repressor vectors to include the tyrosine hydroxylase (TH) and choline acetyltransferase (ChAT) promoters, which are specifically expressed in dopaminergic and cholinergic neurons, respectively. In addition, we introduced an enhanced transcription repressor, the synthetic Krüppel-associated box (KRAB)/methyl CpG binding protein 2 (MeCP2) transcription repression domain (TRD) molecule,⁴¹ to achieve an improved efficacy of the system in reducing *SNCA* expression. Finally, we validated the neuronal-type specificity and efficacy in hiPSC-derived mature neurons, i.e., midbrain dopaminergic neurons (mDAs) and basal forebrain cholinergic neurons (BFCNs), to model PD and DLB, respectively, and assessed the impact on disease-related pathological phenotypes.

RESULTS

Generation and characterization of the neuronal proof-of-concept models

We generated four hiPSC-derived dopaminergic and cholinergic neuronal lines carrying all-in-one LV dCas9-repressor vectors driven by dopaminergic and cholinergic-specific promoters targeted to repress *SNCA* expression and their counterpart control lines. Toward this goal, we constructed two all-in-one LV vectors that contain the guide RNA (gRNA)/dSaCas9 component fused with the synthetic repressor molecule KRAB-MeCP2(TRD), with one driven by the TH promoter (THp-gRNA/dSaCas9/KRAB-MeCP2(TRD); hereafter, THp-Repressor) and the second by the ChAT promoter (ChATp/gRNA/dSaCas9/KRAB-MeCP2(TRD); hereafter, ChATp-Repressor) for specific expression in dopaminergic and cholinergic neurons, respectively (Figure 1A). For each vector, we constructed a control with no gRNA and no repressor (THp-CT and ChATp-CT; Figure 1A). Patients with the triplication of the *SNCA* locus show a constitutively double expression of the *SNCA*-mRNA expression levels and manifest early onset of PD and DLB.^{42–44} Therefore, hiPSC lines derived from a patient with *SNCA* triplication (hereafter, SNCA-Tri) represent adequate models to study PD and DLB in the context of the overexpression of *SNCA*. These four all-in-one LV vectors (THp-Repressor, THp-CT, ChATp-Repressor, ChATp-CT) were transduced into SNCA-Tri hiPSC-derived dopaminergic (MD) and cholinergic (MGE) progenitor neurons to generate a total of eight lines. Four stable transduced MD and four MGE lines were selected and differentiated into dopaminergic neurons (mDAs) and BFCNs, which are primarily affected in PD and DLB, respectively.⁴⁵ To validate successful differentiation, we characterized the neuronal type and differentiation stage of the stably transduced neuronal progenitor cells, MD and MGE, and the fully differentiated mature neurons, mDAs and BFCNs, by real-time RT-PCR and immunocytochemistry using specific markers. The analysis included (1) β -tubulin III (TUBB3), an established marker of prolifer-

ative and terminally differentiated neurons, highly expressed in central nervous system;^{46–48} (2) nestin (NES), a biomarker of neuron progenitor cells;^{49,50} (3) TH, a biomarker for dopaminergic neurons;⁵¹ and (4) ChAT, a marker for cholinergic neurons in the brain as well as the central nervous system.⁵² All lines of the terminally differentiated neurons, mDAs and BFCNs, showed high mRNA expression of TUBB3, while the parental MD and MGE lines did not express TUBB3 as expected (Figures 1B and 1C, left panels). The expression of NES was low in mDAs compared to their parental MD and was nearly undetectable in BFCNs (Figures 1B and 1C, middle panels). The analysis of the neuronal-type-specific markers showed high expression of TH in all mDA lines compared to the corresponding parental MD lines (Figure 1B, right panel) and 27% of the cells expressed TH (Figures 1D and 1E). Similarly, ChAT was strongly expressed in the BFCN lines compared to the parental MGE lines (Figure 1C, right panel) and 30% of the cells were positive to ChAT (Figures 1F and 1G). These results are consistent with our previously published validation studies of the neuronal differentiation protocols showing similar efficiencies of the fully neuronal maturation.^{53,54} In addition, we confirmed co-expression of the all-in-one LV dCas9-repressor vectors in the corresponding matured neuronal lines (Figures 1D and 1F). These findings indicated that all four stably transduced MD lines were successfully differentiated into mDAs and the four stably transduced MGE lines were efficiently differentiated into BFCNs. The evidence of high and specific expression of TH and ChAT in the mDA and BFCN lines, respectively, provided support that the TH and ChAT promoters are effectively active in each specific differentiated neuronal type; thus, each line is expected to effectively express the transduced LV vectors. Collectively, these results demonstrated the establishment of the dopaminergic and cholinergic neuronal models for *in vitro* validation studies of our neuronal-type-specific epigenome-editing system.

Downregulation of *SNCA*-mRNA and protein levels

Previously, we showed that targeted hypermethylation of *SNCA* CpG islands within intron 1 by the catalytic domain of DNMT3A downregulated *SNCA* expression.^{39,40} Here, we studied a new synthetic repressor molecule we recently developed (unpublished data)⁵⁵ composed of KRAB and the TRD domain of MeCP2 and tested its effect on reducing the expression level of the endogenous *SNCA*. We selected a gRNA designed to target the 5' end of intron 1 CpG island known to regulate *SNCA* transcription^{35–37} (Figure 2A). We measured the levels of *SNCA*-mRNA and α -synuclein protein in the four mDA lines and four BFCN lines stably transduced with the THp-Repressor, THp-CT, ChATp-Repressor, and ChATp-CT vectors. In addition, we analyzed the parental progenitor DA and MGE lines and found relatively low levels of *SNCA*-mRNA (Figures 2B and 2C). The mDA line carrying the THp-Repressor vector showed a significant decrease in *SNCA*-mRNA amounting to nearly 50% compared to the mDA control line with the THp-CT vector ($p = 0.0015$, Student's *t* test; Figure 2B, left panel). On the other hand, there was no significant change in *SNCA*-mRNA levels in BFCNs with THp-Repressor vector compared to their control BFCNs with THp-CT line (Figure 2B, right panel), demonstrating the neuronal-type specificity of *SNCA* reduction effect to mDAs.

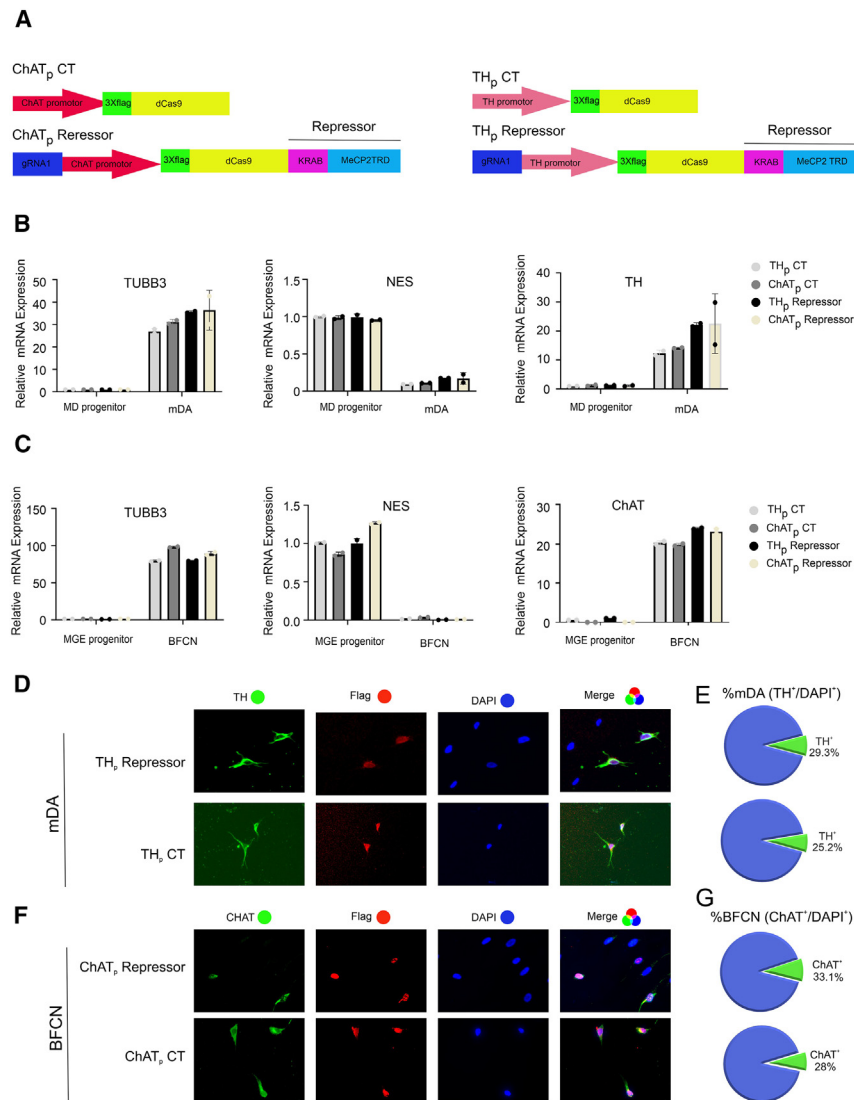


Figure 1. The generation of the hiPSC-derived neuronal proof-of-concept models

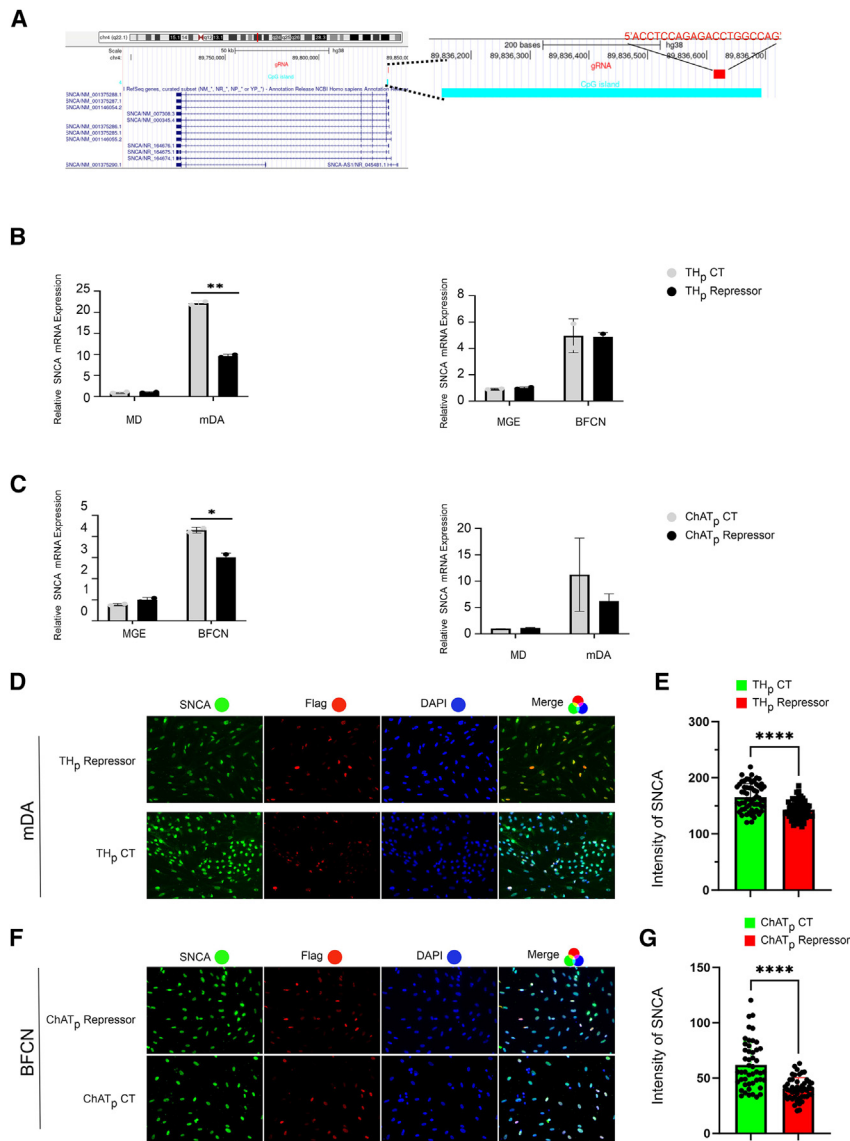
(A) Schematic describing the structure of lentivirus THp-Repressor, THp-CT, ChATp-Repressor, and ChATp-CT vectors. (B) Four stably transduced MD cells were differentiated into final dopaminergic neurons (mDAs). (C) Four stably transduced MGE cells were differentiated into cholinergic neurons (BFCNs). Markers for validation of successful differentiation were evaluated using real-time qRT-PCR for TUBB3 (B and C, left); NES (B and C, middle), TH (B, right), and ChAT (C, right). The levels of mRNAs were measured by TaqMan expression assays and calculated relative to the geometric mean of *GAPDH*-mRNA and *PPIA*-mRNA reference controls using the $2^{-\Delta\Delta CT}$ method. Each column in the data represents the mean value derived from four biological replicates, each of which comprises two technical replicates. The error bars represent the SEM. (D) Representative fluorescence images of the mDA cell lines transduced with THp-Repressor (upper) and -CT (lower) vectors. TH (left), FLAG M2 (middle left), DAPI (middle right), and merge (right). TH, marker of dopaminergic neurons; FLAG M2, tags the all-in-one lentiviral CRISPR-dSaCas9 vectors. (E) Pie charts indicate the percentage of TH⁺ cells (green) out of all cells (DAPI⁺, blue). (F) Representative fluorescence images of the BFCN cell lines transduced with ChAT-Repressor (upper) and -CT (lower) vectors. ChAT (left), FLAG M2 (middle left), DAPI (middle right), and merge (right). ChAT, marker of cholinergic neurons; FLAG M2, tags the all-in-one lentiviral CRISPR-dSaCas9 vectors. (G) Pie charts indicate the percentage of ChAT⁺ cells (green) out of all cells (blue, DAPI⁺).

Next, we evaluated the efficacy of the reduction in the protein levels by immunofluorescence assay using double staining for α -synuclein and M2 FLAG and western blotting. The FLAG marker allowed us to quantify α -synuclein signal intensities directly only in cells in which the THp-Repressor and control vectors were successfully expressed. Quantification analysis of α -synuclein protein was conducted on a subset of mDA cells co-expressing the FLAG at day 21 of the differentiation. The results showed a significant $\sim 30\%$ decrease in α -synuclein protein in the mDAs stably transduced with THp-Repressor vector compared to mDAs with the control THp-CT vector ($p = 0.0002$, Student's *t* test; Figures 2D and 2E). Western blotting analysis validated the significant repression effect on α -synuclein protein ($\sim 40\%$, $p < 0.001$, Student's *t* test; Figures 3A and 3B).

Similar *SNCA* expression analyses were carried out for the ChATp lines. We observed $\sim 30\%$ lower levels of *SNCA*-mRNA in BFCNs car-

rying the ChATp-Repressor compared to ChATp-CT vectors ($p = 0.0174$, Student's *t* test; Figure 2C, left panel), while there was no effect on *SNCA*-mRNA levels in the mDAs with the ChATp-Repressor vector vs. the control mDAs (Figure 2C, right panel). Thus, the *SNCA* repression effect of ChATp-Repressor was specific to BFCNs. Next, we analyzed the effect on α -synuclein protein level. Immunofluorescent analysis of the FLAG-co-expressing BFCNs cells at day 21 of the differentiation validated a significant reduction in the endogenous α -synuclein levels by approximately 20% in the BFCNs with the ChATp-Repressor vector vs. the control ChATp-CT vector ($p = 0.004$, Student's *t* test; Figures 2F and 2G). Western blotting analysis confirmed the significant repression effect on α -synuclein protein level ($\sim 44\%$, $p = 0.0419$, Student's *t* test; Figures 3E and 3F).

Our first-generation ectopic-expressed system driven by a constitutive promoter demonstrated a minimal off-target effect.³⁹ Here we examined the target specificity of the novel neuronal-type-specific system harboring our engineered transcription-repressor molecule by a comprehensive gene expression analysis using TaqMan array. Since the effector molecule directly represses transcription, we analyzed the expression of 32 random genes by qRT-PCR. Our results showed



ChATp-CT as identified by FLAG co-expression. The quantification analysis was performed three times independently, and each time 50 co-expressed cells per BFCN line were analyzed. * $p < 0.02$, ** $p < 0.005$, or *** $p < 0.0002$; Student's *t* test.

similar gene expression profiles for most tested genes in all transduced (repressor and control vectors) and naive mDAs and BFCN cell lines (Figure S1). Notably, the expression of *CDKN1A* and *PES1* genes was significantly reduced in the BFCN line transduced with the no-gRNA/no-repressor vector compared to the cells with the vector harboring the gRNA repressor (Figure S1). These results further supported the specificity and accuracy of the effect of the vectors containing the gRNA-repressor component on *SNCA*-mRNA expression.

Collectively, the effects of the all-in-one LV THp-Repressor and ChATp-Repressor vectors were consistent on the mRNA and protein levels in the mDAs and BFCNs, respectively. Overall, these data demonstrated consistently the efficacy and specificity of the THp-

Repressor and the ChATp-Repressor vectors on repressing *SNCA* expression in dopaminergic and cholinergic neurons, respectively.

The effect of the neuronal-type-specific *SNCA* transcriptional repressor on disease-related cellular phenotypes

The predominant post-translational modification of α -synuclein in LBs is phosphorylation at serine (Ser)129, a marker of the pathological α -synuclein aggregates, which is a hallmark of synucleinopathies.^{56,57}

Thus, to determine the effect of the reduction in α -synuclein levels mediated by our system on ameliorating disease-related neuropathological characteristics, we analyzed the reactivity to Ser129 phosphorylation of α -synuclein (pS129- α -synuclein) in the stably transduced mDA and BFCN lines by western blotting. Fully differentiated (day

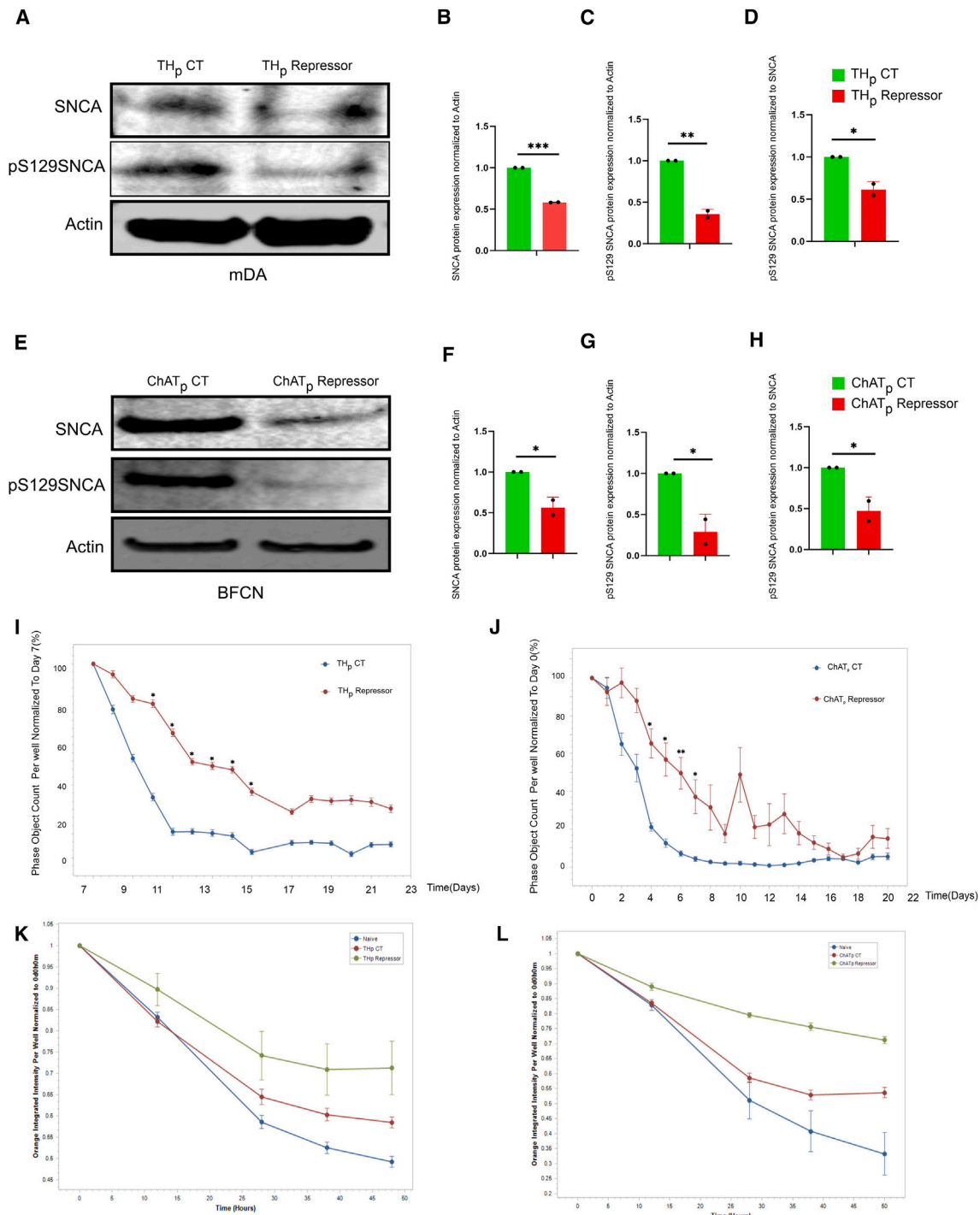


Figure 3. The effects of the neuronal-type-specific repression of SNCA overexpression on α -synuclein aggregates, cell viability, and mitochondria function

(A) Representative western blot of α -synuclein and pS129- α -synuclein in mDAs stably transduced with THp-Repressor compared to THp-CT. (B–D) Quantitative analyses of total α -synuclein protein (B) and pS129- α -synuclein protein (C) normalized to B-actin, and of pS129- α -synuclein normalized to total α -synuclein expression (D) in mDA cells. (E) Representative western blot of α -synuclein and pS129- α -synuclein in BFCNs stably transduced with ChATp-Repressor compared to ChATp-CT. (F–H) Quantitative analyses of total α -synuclein protein (F) and pS129- α -synuclein protein (G) normalized to B-actin, and of pS129- α -synuclein normalized to total α -synuclein expression (H) in BFCN cells. * $p < 0.05$, ** $p < 0.01$, or *** $p < 0.001$; Student's t test. (I and J) Cell viability assay using the Incucyte S3 live-cell analysis system. Plots were generated using the built-in software. (I) The effect of the THp-Repressor vector (red) compared to the respective control vector (THp-CT, blue) on cell viability in mDAs during the differentiation

(legend continued on next page)

21) mDAs carrying the THp-Repressor vector showed significantly lower levels of pS129- α -synuclein compared to the control mDA line ($\sim 60\%$, $p = 0.0041$, Student's t test; Figures 3A and 3C). In order to control for the effect of the overall decrease in α -synuclein level (Figures 3A and 3B), we determined the ratios of pS129- α -synuclein/total α -synuclein. The ratio found for the mDAs with the THp-Repressor vector was significantly lower in comparison to the control ($\sim 40\%$, $p = 0.0305$, Student's t test; Figures 3A and 3D). Thus, the decreased level of pS129- α -synuclein was greater than the overall reduction in α -synuclein, suggesting that our epigenome therapy system rescued the pathological surrogate marker of α -synuclein aggregates. Similarly, the levels of pS129- α -synuclein in the mature BFCNs carrying the ChATp-Repressor vector were significantly decreased compared to the control BFCNs ($\sim 70\%$, $p = 0.0425$, Student's t test; Figures 3E and 3G). Upon normalization to total α -synuclein, the reduction remained substantial, showing a significantly lower pS129- α -synuclein/total α -synuclein ratio in the BFCNs with the ChATp-Repressor vector vs. the control line ($\sim 50\%$, $p = 0.0462$, Student's t test; Figures 3E and 3H), indicating the rescue of the surrogate marker of α -synuclein aggregates.

The neurotoxicity effects of elevated levels of α -synuclein have been well established and numerous reports demonstrated the relationship between SNCA overexpression and neuronal cell death.²⁵ To understand the effect of the decrease in α -synuclein levels mediated by our system on neuronal cell loss, we performed a cell viability assay over a period of 21 days using the IncuCyte S3 system. This technology allows for real-time, continuous monitoring of cell growth and health by utilizing an imaging platform to quantify the number of live cells in a culture.

The MD cells stably transduced with THp-Repressor and THp-CT and the MGE cells stably transduced with ChATp-Repressor and ChATp-CT were placed in the IncuCyte S3 system, and images were taken at every 24 h for 21–22 days, during which the differentiation protocols were applied. The images were analyzed using the IncuCyte software, which automatically quantifies the number of live cells based on their morphological features. The results showed a higher cell viability in the MD line carrying the THp-Repressor vector compared to MD with the control vector from day 7 and throughout the differentiation process to mature mDA neurons (Figure 3I), reaching statistical significance in days 11–15 (Table S4). On day 15 of the differentiation, more than 40% of the dopaminergic neurons with the THp-Repressor vectors were viable, while the viability of the control neurons was significantly lower ($p = 0.013052$, Student's t

test; Table S4). At the end of the experimental period (day 22), $\sim 30\%$ of the THp-Repressor stable transduced dopaminergic neurons remained viable (Figure 3I). Similar results were found with the cholinergic lines, demonstrating a higher level of viable cells for the MGE carrying the ChATp-Repressor vector compared to the corresponding control cells along the differentiation process to mature BFCNs (Figure 3J), showing significant differences on days 4–7 (Table S5). At day 6, the control cholinergic neurons already exhibited the lowest cell viability value compared to $\sim 50\%$ viability at day 6 for the cholinergic neurons with the ChATp-Repressor ($p = 0.001$, Student's t test; Figures 3J and Table S5). Noteworthy, only at day 16 did the ChATp-Repressor cholinergic neurons show a comparable low level of viable cells to that observed for the control ChATp-CT cholinergic neuronal line at day 6 (Figure 3J). These findings are consistent with the significant differences in viable cells between these lines. Together, these results suggested that downregulation of SNCA mediated by our epigenome-editing system enhanced dopaminergic and cholinergic neuronal survival during the differentiation process.

Mitochondrial dysfunction has been implicated in driving the pathology of several neurodegenerative diseases, including PD and DLB, and the association between overexpression of α -synuclein and dysfunctional mitochondria has been established.⁵⁸ To explore the beneficial effect of α -synuclein downregulation mediated by our system on mitochondrial function, we conducted the IncuCyte mitochondrial membrane potential (MMP) assay at day 10 of the differentiation process. A drop in MMP indicates a disruption in mitochondrial function and integrity. The MMP assay utilizes the IncuCyte MMP Orange Reagent, which accumulated in active mitochondria in proportion to the MMP and by that enables real-time detection of transient and long-term changes in MMP in live cells. The control THp-CT dopaminergic and ChATp-CT cholinergic neuronal lines demonstrated a robust decrease in the orange fluorescence intensity compared to their counterpart neuronal lines stably transduced with the THp-Repressor and the ChATp-Repressor, respectively (Figures 3K and 3L). The results showed similar decline trends in the orange fluorescence intensities for the control and the naive cells of each neuronal type over a period of 28 h (Figures 3K and 3L). Thus, the MMP remained more stable in the THp-Repressor dopaminergic and the ChATp-Repressor cholinergic neurons relative to the drops observed in monitoring the respective naive and control neuronal lines (Figures 3K and 3L). These results indicated that our epigenome therapy system ameliorated mitochondrial dysfunction and perturbed integrity in dopaminergic and cholinergic disease model neurons.

process from MD cell lines. (J) The effect of the ChATp-Repressor vector (red) compared to the respective control vector (ChATp-CT, blue) on cell viability in BFCNs during the differentiation process from MGE cell lines. The assay was performed three times for each line. * $p < 0.05$, ** $p < 0.01$, or *** $p < 0.001$; multiple Student's t test. (K and L) Mitochondrial membrane potential (MMP) analysis using the IncuCyte Sx5 live-cell analysis system. Cells were monitored along a period of 48 h at day 10 of the differentiation into mDAs (K) and BFCNs (L). Plots were generated using the built-in software. (K) Quantification of the orange fluorescence intensities the mDA lines stably transduced with THp-Repressor vector (green), the respective control vector (THp-CT, red), and the naive cells (blue). The THp-Repressor vector rescued the loss of MMP observed in the THp-CT and naive neuronal lines. (L) Quantification of the orange fluorescence intensities the BFCN lines stably transduced with ChATp-Repressor vector (green), the respective control vector (ChATp-CT, red), and the naive cells (blue). The ChATp-Repressor vector rescued the loss of MMP observed in the THp-CT and naive neuronal lines. The assay was performed three times for each line.

Collectively, the results demonstrated that the epigenome-editing-mediated neuronal-type-specific reduction in *SNCA*-expression levels reversed the phenotypic perturbations of the *SNCA*-Tri hiPSC-derived dopaminergic and cholinergic neurons.

DISCUSSION

In this study, we developed the first cell-type-specific *SNCA*-targeted epigenome-editing tool applicable as a gene therapy approach for synucleinopathy spectrum disorders. Specifically, we developed a novel all-in-one LV vector harboring gRNA, dCas9, and the fused KRAB-MeCP2(TRD) repressor molecule driven by TH and ChAT promoters to precisely target a regulatory element within *SNCA* intron 1 region with specificity to dopaminergic and cholinergic neurons, respectively. Validation of the neuronal-specific epigenome-editing system, using mDA and BFCN mature neurons derived from a patient with *SNCA* triplication, resulted in neuronal-type-specific downregulation of *SNCA*-mRNA and protein expression. Moreover, as a consequence, the neuronal-type-specific *SNCA* reduction rescued disease-related pathological hallmarks, in particular neuronal survival, mitochondrial dysfunction, and the levels of Ser129-phosphorylated α -synuclein, the predominant modification of α -synuclein in the pathological aggregates.⁵⁶

In previous studies, we developed the first generation of the technology.^{39,40} Here, we aimed to refine the system for therapeutics applications specific for each synucleinopathy (i.e., PD and DLB). Toward this goal, we developed a new improved system and perfected the platform several ways. Foremost, the prior viral vector was expressed from a constitutive promoter (EF1 α core promoter [EFS-NC]). To achieve efficient and specific expression of the system in the vulnerable neuronal types for each disease, we modified the promoter to TH and ChAT, specific markers of dopaminergic and cholinergic neurons, respectively. This modification also circumvents undesirable manipulation of *SNCA* expression in other cell types. Thus, it facilitates the assessment of route of administration (ROA) that are not directed into the affected brain region, such as intracerebroventricular (ICV) and the non-invasive intranasal drug delivery routes to the brain. In addition, we engineered a novel synthetic repressor protein based on the fusion of KRAB and the TRD of MeCP2, which demonstrated a stronger efficacy to reduce expression (our unpublished data).⁵⁵ Another improvement of the engineered KRAB-MeCP2(TRD) is the smaller size relative to DNMT3A. Finally, we replaced the deactivated nuclease to the compact *Staphylococcus aureus* (*Sa*)Cas959. Overall, the new all-in-one vector that includes d*Sa*Cas9/KRAB-MeCP2(TRD) can be packaged in the payload-limited adeno-associated viral (AAV) vector that is commonly used for *in vivo* gene editing⁵⁹ (our unpublished data). Collectively, the new system brings crucial advancements and strengthens the translational potential for precision medicine in synucleinopathies.

In this proof-of-concept study, we validated the new all-in-one d*Sa*-Cas9/KRAB-MeCP2(TRD) using hiPSC-derived mDA and BFCN lines obtained from a patient carrying the triplication of the *SNCA*

locus (*SNCA*-Tri hiPSC). Patients with the *SNCA* triplication manifest early-onset PD and DLB;⁴² therefore, hiPSC lines obtained from these patients represent an adequate model for PD and DLB drug discovery and preclinical studies.^{39,40,53} Application of hiPSC-derived systems as disease models for drug discovery has become increasingly common,^{60,61} specifically in early preclinical phase to explore the cellular disease pathophysiology and validate drug targets and as screening and optimization platforms of early therapeutics strategies (reviewed in MacDougall et al.⁶⁰). hiPSC-derived disease models are beneficial in preclinical phase for several reasons; primarily, they represent the only available human-based models in which the full genetic landscape of the patients is captured.⁶⁰ In addition, they are cost-effective, versatile, and overcome many of the innate limitations of available animal models.⁶⁰ We recently performed in-depth characterization of *SNCA*-Tri hiPSC-derived mDAs and BFCNs provided further support for their suitability to model PD and DLB, respectively, for basic, translational, and preclinical studies.⁵³ Our current preclinical study demonstrated the utility and feasibility of patient hiPSC-derived neuronal models in the early stage of drug development and provided evidence for the importance of hiPSC technology in offering the opportunity to perform validation studies using the relevant cell type for each disease indication.

Manipulations of *SNCA* levels have demonstrated a beneficial impact.^{31–33} However, neurotoxicity associated with robust reduction of *SNCA* levels was reported.^{62,63} Familial patients with the triplication or duplication of the *SNCA* locus showed constitutively 200% and 150% higher levels of *SNCA*,^{42–44,53} respectively, compared to subjects with diploid copies of *SNCA*, and these patients manifest early-onset PD and DLB.^{42,44} Thus, it is predicted that a reduction of 33%–50% in *SNCA*-mRNA and protein expression should restore normal physiological levels of *SNCA* and be sufficient for therapeutic benefits. Our goal is to fine-tune *SNCA* levels in sporadic PD and DLB caused by *SNCA* dysregulation, and we presume that a reduction of 30% or less could serve as the therapeutic window. Here, we achieved neuronal-type-specific reduction in *SNCA* overexpression of 41% and 44% in dopaminergic and cholinergic neurons, respectively. Furthermore, we demonstrated that these reduction levels were sufficient to effectively reverse key neuropathological features (i.e., the presence Ser129-phosphorylated α -synuclein, surrogate of α -synuclein aggregates, neuronal cell loss, and mitochondrial dysfunction). These results provided an *in vitro* proof of concept for the efficacy and efficiency of our new neuronal-type-specific therapeutic strategy and a strong premise for moving forward into animal studies toward IND enablement.

In conclusion, our new *SNCA*-targeted epigenome therapy presents a strategy for targeting the precise gene in the precise brain-cell-type in the affected brain region. The platform offers the opportunity to refine the vector for packaging in AAV for safer and efficient delivery into the brain. This study introduces PD- and DLB-specific gene therapy technologies and thereby advances precision medicine in synucleinopathies.

MATERIALS AND METHODS

Plasmid design and construction

The triple-FLAG-tagged KRAB-MeCP2(TRD) repressor was amplified from pCL52 and cloned into a lentivirus vector carrying dSa-Cas9-p2a-puromycin with an effector cloning site under the control of EF-1a promoter and a gRNA-cloning site (two BsmBI cutting sites) located downstream of the U6 promoter. The EF-1a promoter was then replaced with human TH promoter and human choline acetyltransferase (ChAT) promoter to generate two separate neuronal-type-specific vectors. Next, the p2A sequence was replaced with SV40 promoter to support the expression of the puromycin resistance gene in the selection of the neural progenitor cells. The gRNA sequence (gRNA1, ACCTCCCAGAGACCTGGCCCAG) targeting the *SNCA* gene was inserted into the two BsmBI sites. The resulting vectors were named TH_p-Repressor and ChAT_p-Repressor, respectively. To generate the negative-control vectors, the vectors without gRNAs were used and the KRAB-MeCP2(TRD) cassette was removed by digestion with AgeI and FseI, resulting in negative-control plasmid TH_p-CT and ChAT_p-CT, respectively. The cell-type-specific promoters (TH and ChAT promoter) were synthesized using the GenScript Biotech (Piscataway, NJ) service.

Lentiviral particle production

LVs were generated using the transient transfection protocol,⁶⁴ as described previously. Briefly, 15 µg of vector plasmid, 10 µg of psPAX2 packaging plasmid (Addgene 12260), 5 µg of pMD2.G envelope plasmid (Addgene 12259), and 2.5 µg of pRSV-Rev plasmid (Addgene 12253) were transfected into 293T cells. Vector particles were collected from filtered conditioned medium at 72 h post transfection. The particles were purified using the sucrose-gradient method and concentrated >250-fold by ultracentrifugation (2 h at 20,000 rpm). Vector and viral stocks were aliquoted and stored at -80°C.

Transduction and puromycin selection

MD and MGE were transduced with each of the constructed LV repressor and control vectors at the MOI = 0.2. At 16 h post-transduction, the media were replaced, and, at 48 h post transduction, puromycin was applied at the final concentration of 1 µg/mL. The cells were maintained on the puromycin selection medium for 21 days to obtain the stable MD and MGE lines that carry each of the different LV repressor and control vectors.

Cell culture and neuronal differentiation

hiPSCs from a patient with a triplication of the *SNCA* gene (*SNCA*-Tri, ND34391, RRID:CVCL_F202) was purchased from the National Institute of Neurological Disorders and Stroke (NINDS) Human Cell and Data Repository (<https://nindsgenetics.org>). The ND34391 line was previously differentiated into progenitor neurons, ventral midbrain (MD) and medial ganglionic eminence (MGE)⁴⁵ as described in Tagliafierro et al.⁵³

Differentiation of MD into mDAs was performed following the following protocol.^{53,65} Briefly, 5×10^5 cells/mL MD were seeded

on poly-L-ornithine/laminin-coated plates in N2B27 medium supplemented with 3 µM CHIR99021, 2 µM SB431542, 5 µg/mL BSA, 20 ng/mL fibroblast growth factor (FGF), and 20 ng/mL epidermal growth factor (EGF). At 24 h post passage, MD maintenance medium was substituted by final differentiation medium consisting of N2B27 medium supplemented with 100 ng/mL FGF8 (Peprotech), 2 µM purmorphamine, 300 ng/mL dibutyryl-cyclic AMP (cAMP) (db-cAMP), and 200 µM L-ascorbic acid (L-AA) for 14 days. From day 14, cells were fed with maturation medium consisting of 20 ng/mL glial cell line-derived neurotrophic factor (GDNF), 20 ng/mL Brain-derived neurotrophic factor (BDNF), 10 µM DAPT, 0.5 mM db-cAMP, and 200 µM L-AA. Medium was changed every other day.

Differentiation of MGE into BFCNs was performed with the following protocol.^{53,66} Briefly, 5×10^5 cells/mL MGE were seeded on poly-L-ornithine/laminin-coated plates in NEM (seven parts KO-DMEM to three parts F12, 2 mM Glutamax, 1% penicillin and streptomycin, supplemented with 2% B27), plus 20 ng/mL FGF, 20 ng/mL EGF, 5 µg/mL heparin, 20 µM SB431542, and 10 µM Y27632 medium supplemented with 3 µM CHIR99021, 2 µM SB431542, 5 µg/mL BSA, 20 ng/mL bFGF, and 20 ng/mL. At 24 h post passage, MGE maintenance medium was substituted by final differentiation medium, BrainPhys Medium (Stemcell Technologies) supplemented with N2, B27, BDNF, GDNF, L-ascorbic acid, and db-cAMP for 3 weeks. Medium was changed every other day.

Cell count assay

To determine the differentiation efficiency of MD into mDAs and MGE into BFCNs, fluorescence images were collected using an EVOS microscope. The numbers of total cell (DAPI⁺), mDA(TH⁺), and BFCN(ChAT⁺) were counted manually. Total differentiation efficiency of MGE/MD was assessed by the ratio of TH⁺ cells or ChAT⁺ and DAPI labeling cells. From each coverslip, five randomly chosen fields were counted.

RNA extraction and cDNA synthesis

For this, 3×10^5 cells were grown in cell differential medium for neuron differentiation. At day 21, cell samples were harvested and total RNA was extracted and purified from cells using Total RNA Purification Kits (Norgen Biotek, Canada). RNA concentration was determined spectrophotometrically at 260 nm using Nanodrop One Spectrophotometer (Thermo Scientific), while the quality of the purification was determined by 260/280 nm ratio, which showed values between 1.9 and 2.1, indicating high RNA quality. cDNA was synthesized using SuperScript IV VILO Master Mix (Thermo Scientific) according to the manufacturer's manual.

Real-time PCR

Real-time PCR was used to quantify the mRNAs expression of the neuronal markers and to evaluate possible off-target effects. Quantification of neuronal markers was performed as previously described.^{53,54} Briefly, triplicates of each sample were assayed by relative real-time qPCR using TaqMan expression assays and the ABI QuantStudio 7 (Applied Biosystems) to determine the level of

the mRNA of the neuronal markers in the different cell lines relative to mRNAs encoding housekeeping genes. The TaqMan minor groove binder (MGB) probe and primer set assays (Applied Biosystems) were used to amplify the target neuronal markers and the housekeeping reference controls are listed in Table S1. Each cDNA (5 ng) was amplified in duplicate in at least two independent runs (≥ 4 repeats overall), using TaqMan Fast Advanced Master Mix reagent (Applied Biosystems) and the following conditions: 2 min at 50°C, 10 min at 95°C, 40 cycles; 15 s at 95°C; and 1 min at 60°C. Data were analyzed using a comparative delta-delta Ct method, also known as the 2- $\Delta\Delta$ Ct method. The cycle number at which any sample crossed that threshold (Ct) was then used to determine fold difference, whereas the geometric mean of the two control genes served as a reference for normalization. Fold difference was calculated as $2^{-\Delta\Delta\text{Ct}}$. $\Delta\text{Ct} = [\text{Ct}(\text{target}) - \text{Ct}(\text{geometric mean of reference})]$. $\Delta\Delta\text{Ct} = [\Delta\text{Ct}(\text{sample})] - [\Delta\text{Ct}(\text{calibrator})]$. The calibrator was a particular RNA sample obtained either from human total brain RNA (Thermo Scientific) or control cells, used repeatedly in each plate for normalization within and across runs. The variation of the ΔCt values among the calibrator replicates was smaller than 10%.

Off-target analysis was performed using a commercial array (Applied Biosystems) consisting of 32 genes (*18S*, *GADPH*, *HPRT1*, *GUSB*, *ACTB*, *B2M*, *HMBS*, *IPO8*, *PGK1*, *RPLPO*, *TBP*, *TFRC*, *UBC*, *YWHAZ*, *PPIA*, *POLR1A*, *CASC3*, *CDKN1A*, *CDKN1B*, *GADD45A*, *PUM1*, *PSMC4*, *EIF2B1*, *PES1*, *ABL1*, *ELF1*, *MT-AT6*, *MRPL19*, *POP4*, *RPL37A*, *RPL30*, *RPS17*). Data were uploaded to the Thermo Fisher Cloud and analyzed with Applied Biosystems qPCR Analysis Modules.

Immunocytochemistry

For imaging, 2.6×10^4 cells were plated onto Nunc Lab-Tek Chamber Slide System (Thermo Scientific). Cells were fixed in 4% paraformaldehyde (PFA) and permeabilized in 0.1% Triton X-100 prior to immunofluorescence staining. Cells were then blocked in 5% goat serum for 1 h before incubating with primary antibodies overnight at 4°C. Following washes with PBS, cells were incubated with secondary antibodies (Alexa Fluor, Life Technologies) for 1 h at room temperature. Nuclei were stained with NucBlue Fixed Cell ReadyProbes Reagent (Thermo Fisher), following the manufacturers' instructions. Images were captured on EVOS (Invitrogen). Primary and secondary antibodies are listed in Table S2.

For the quantitative analysis of immunofluorescence, 50 cells from each mDA/BFCN lines were imaged. The immunofluorescence intensity of α -synuclein protein and the FLAG were measured using ImageJ software. The percentage of successfully differentiated mDAs and BFCNs was determined by the number of TH-positive and ChAT-positive cells, respectively, divided by the total number of DAPI-positive cells.

Western blotting

Here, 2×10^6 cells were grown in cell differential medium for neuron differentiation. At day 21, cell samples were harvested and

lysed with RIPA buffer (Millipore, Germany). Expression levels of the total human α -synuclein protein and the Ser129 phosphorylated α -synuclein protein (pS129- α -synuclein) in the mDA/BFCN lines were determined by western blotting with the α -synuclein rabbit monoclonal antibody (1:2,000), pS129- α -synuclein polyclonal antibody (1:500), and with monoclonal antibody (mAb) B-actin (1:5,000) for normalization. The list of antibodies used for the western blotting can be found in Table S3. The cells were scraped from the dish and homogenized in RIPA buffer (EMD Millipore, MA) in the presence of a protease and phosphatase repressor cocktail (Sigma, St. Louis, MO). Total protein concentrations were determined by the BCA Protein Assay (Thermo Scientific), and 25 mg of each sample was run on 4%–12% NuPAGE gels. Proteins were transferred to polyvinylidene fluoride (PVDF) membranes, and blots were first incubated with 0.4% paraformaldehyde (PFA) and then blocked with Blocker FL Fluorescent Blocking Buffer (Thermo Scientific). Primary antibodies were incubated at 4°C overnight. Alexa Fluor 790 donkey anti-rabbit IgG- and Alexa Fluor 680 donkey anti-mouse IgG-conjugated secondary antibodies were incubated for 1 h at room temperature (Abcam; 1:10,000). The signal was detected and imaged using the iBright system (Thermo Scientific). Total α -synuclein and pS129- α -synuclein expression was normalized to B-actin expression in the same lane. Relative pS129- α -synuclein was normalized to total α -synuclein in the same line. Each experiment was repeated twice.

Cell viability

mDA/BFCN differentiation assays were carried out as described above. Briefly, 2.5×10^5 indicated cell lines were cultured in differentiation medium for 4 days and then placed in Incucyte S3 (Sartorius, Germany), a simple, reliable, and easy method through the Incucyte S3 live-cell analysis system for cell viability assay,^{67–69} for over time image acquisition. The plate was scanned from nine separate regions per well using a 20 \times objective lens every 24 h for 21 days. The images were then analyzed using the built-in tools, and the viable cell number (object count) changes over time, normalized to the indicated day, were plotted using the built-in software.

MMP analysis

Changes in the MMP of the differentiated mDA and BFCN cells were analyzed using Incucyte MMP Orange Reagent Kit (Sartorius, Germany), and 2.5×10^4 MD cells stably transduced with THp-Repressor and THp-CT and the MGE cells stably transduced with ChATp-Repressor and ChATp-CT were cultured in poly-ornithine/laminin-coated 96-well plates with differentiation medium. At day 10, cells were incubated with culture medium containing 20 nM Incucyte MMP Orange Reagent for 1 h and then placed in an Incucyte Sx5 (Sartorius, Germany) for imaging. Cells exhibiting orange fluorescing mitochondria were considered healthy. The images were analyzed with the Incucyte Basic Analysis Software Module.

Statistical analyses

Each RT-PCR experiment was repeated four times. The immunofluorescence assay, western blotting assay, cell viability assay, and MMP

assay were repeated three times each to ensure accuracy and reproducibility.

All data are presented as mean \pm standard error of the mean (SEM). Error bars in figures represent SEM to visualize data variability. The significance of the differences between the mean values were analyzed by the two-tailed unpaired Student's *t* test using GraphPad Prism 9. To perform statistical analysis on the cell viability assay, the raw data were exported from the Incucyte instrument, and the values of arguments "Area" were used to perform multiple *t* tests. *p* values \leq 0.05 were considered to indicate statistically significant differences.

DATA AND CODE AVAILABILITY

All data collected for this study and LV vector sequences will be available upon publication under controlled-use conditions as [supplemental information](#) and/or via a website link.

SUPPLEMENTAL INFORMATION

Supplemental information can be found online at <https://doi.org/10.1016/j.omtn.2023.102084>.

ACKNOWLEDGMENTS

This work was funded in part by the National Institutes of Health/National Institute of Neurological Disorders and Stroke (NIH/NINDS) (RF1 NS113548-01A1 to O.C.-F.) and by a grant from Seelos Therapeutics, Inc. to CLAIRGene, LLC.

AUTHOR CONTRIBUTIONS

O.C.-F. conceptualized the original idea. Z.S., B.K., and O.C.-F. designed the experimental plan and performed the analysis and interpretation of the data. Z.S. carried out the experiments. B.K. and O.C.-F. supervised the project and acquired funding. Z.S. prepared the figures and tables. Z.S., B.K., and O.C.-F. wrote the manuscript. All authors reviewed the manuscript.

DECLARATION OF INTERESTS

Drs. Chiba-Falek and Kantor are inventors of intellectual property related to this research, and Duke University filed a patent application for the technology developed in this study. CLAIRGene has an exclusive, worldwide option agreement from Duke for the related patent portfolio for all fields of use. Dr. Sun is a scientist at CLAIRGene. Drs. Kantor and Chiba-Falek are co-founders at CLAIRGene, LLC.

REFERENCES

- Galvin, J.E., Lee, V.M., and Trojanowski, J.Q. (2001). Synucleinopathies: clinical and pathological implications. *Arch. Neurol.* *58*, 186–190.
- Martí, M.J., Tolosa, E., and Campdelacreu, J. (2003). Clinical overview of the synucleinopathies. *Mov. Disord.* *18* (Suppl 6), S21–S27.
- Spillantini, M.G. (1999). Parkinson's disease, dementia with Lewy bodies and multiple system atrophy are alpha-synucleinopathies. *Parkinsonism Relat. Disord.* *5*, 157–162.
- Jellinger, K.A. (2003). Neuropathological spectrum of synucleinopathies. *Mov. Disord.* *18* (Suppl 6), S2–S12.
- Spillantini, M.G., Schmidt, M.L., Lee, V.M., Trojanowski, J.Q., Jakes, R., and Goedert, M. (1997). Alpha-synuclein in Lewy bodies. *Nature* *388*, 839–840.
- Cookson, M.R. (2005). The biochemistry of Parkinson's disease. *Annu. Rev. Biochem.* *74*, 29–52.
- Dawson, T.M., and Dawson, V.L. (2003). Molecular pathways of neurodegeneration in Parkinson's disease. *Science* *302*, 819–822.
- Braak, H., Del Tredici, K., Rüb, U., de Vos, R.A.I., Jansen Steur, E.N.H., and Braak, E. (2003). Staging of brain pathology related to sporadic Parkinson's disease. *Neurobiol. Aging* *24*, 197–211.
- Grothe, M.J., Schuster, C., Bauer, F., Heinsen, H., Prudlo, J., and Teipel, S.J. (2014). Atrophy of the cholinergic basal forebrain in dementia with Lewy bodies and Alzheimer's disease dementia. *J. Neurol.* *261*, 1939–1948.
- Hall, H., Reyes, S., Landeck, N., Bye, C., Leanza, G., Double, K., Thompson, L., Halliday, G., and Kirik, D. (2014). Hippocampal Lewy pathology and cholinergic dysfunction are associated with dementia in Parkinson's disease. *Brain* *137*, 2493–2508.
- Marui, W., Iseki, E., Nakai, T., Miura, S., Kato, M., Ueda, K., and Kosaka, K. (2002). Progression and staging of Lewy pathology in brains from patients with dementia with Lewy bodies. *J. Neurol. Sci.* *195*, 153–159.
- Beach, T.G., Adler, C.H., Lue, L., Sue, L.I., Bachalakuri, J., Henry-Watson, J., Sasse, J., Boyer, S., Shirohi, S., Brooks, R., et al. (2009). Unified staging system for Lewy body disorders: correlation with nigrostriatal degeneration, cognitive impairment and motor dysfunction. *Acta Neuropathol.* *117*, 613–634.
- Pankratz, N., Wilk, J.B., Latourelle, J.C., DeStefano, A.L., Halter, C., Pugh, E.W., Doheny, K.F., Gusella, J.F., Nichols, W.C., Foroud, T., et al. (2009). Genomewide association study for susceptibility genes contributing to familial Parkinson disease. *Hum. Genet.* *124*, 593–605.
- Myhre, R., Toft, M., Kachergus, J., Hulihan, M.M., Aasly, J.O., Klungland, H., and Farrer, M.J. (2008). Multiple alpha-synuclein gene polymorphisms are associated with Parkinson's disease in a Norwegian population. *Acta Neurol. Scand.* *118*, 320–327.
- Ross, O.A., Gosal, D., Stone, J.T., Lincoln, S.J., Heckman, M.G., Irvine, G.B., Johnston, J.A., Gibson, J.M., Farrer, M.J., and Lynch, T. (2007). Familial genes in sporadic disease: common variants of alpha-synuclein gene associate with Parkinson's disease. *Mech. Ageing Dev.* *128*, 378–382.
- Pals, P., Lincoln, S., Manning, J., Heckman, M., Skipper, L., Hulihan, M., Van den Broeck, M., De Pooter, T., Cras, P., Crook, J., et al. (2004). alpha-Synuclein promoter confers susceptibility to Parkinson's disease. *Ann. Neurol.* *56*, 591–595.
- Mueller, J.C., Fuchs, J., Hofer, A., Zimprich, A., Lichtner, P., Illig, T., Berg, D., Wüllner, U., Meitinger, T., and Gasser, T. (2005). Multiple regions of alpha-synuclein are associated with Parkinson's disease. *Ann. Neurol.* *57*, 535–541.
- Mizuta, I., Satake, W., Nakabayashi, Y., Ito, C., Suzuki, S., Momose, Y., Nagai, Y., Oka, A., Inoko, H., Fukae, J., et al. (2006). Multiple candidate gene analysis identifies alpha-synuclein as a susceptibility gene for sporadic Parkinson's disease. *Hum. Mol. Genet.* *15*, 1151–1158.
- Winkler, S., Hagenah, J., Lincoln, S., Heckman, M., Haugarvoll, K., Lohmann-Hedrich, K., Kostic, V., Farrer, M., and Klein, C. (2007). {alpha}-Synuclein and Parkinson disease susceptibility. *Neurology* *69*, 1745–1750.
- Satake, W., Nakabayashi, Y., Mizuta, I., Hirota, Y., Ito, C., Kubo, M., Kawaguchi, T., Tsunoda, T., Watanabe, M., Takeda, A., et al. (2009). Genome-wide association study identifies common variants at four loci as genetic risk factors for Parkinson's disease. *Nat. Genet.* *41*, 1303–1307.
- Simón-Sánchez, J., Schulte, C., Bras, J.M., Sharma, M., Gibbs, J.R., Berg, D., Paisan-Ruiz, C., Lichtner, P., Scholz, S.W., Hernandez, D.G., et al. (2009). Genome-wide association study reveals genetic risk underlying Parkinson's disease. *Nat. Genet.* *41*, 1308–1312.
- Maraganore, D.M., de Andrade, M., Elbaz, A., Farrer, M.J., Ioannidis, J.P., Krüger, R., Rocca, W.A., Schneider, N.K., Lesnick, T.G., Lincoln, S.J., et al. (2006). Collaborative analysis of alpha-synuclein gene promoter variability and Parkinson disease. *JAMA* *296*, 661–670.
- Nalls, M.A., Pankratz, N., Lill, C.M., Do, C.B., Hernandez, D.G., Saad, M., DeStefano, A.L., Kara, E., Bras, J., Sharma, M., et al. (2014). Large-scale meta-analysis of genome-wide association data identifies six new risk loci for Parkinson's disease. *Nat. Genet.* *46*, 989–993.

24. Bras, J., Guerreiro, R., Darwent, L., Parkkinen, L., Ansorge, O., Escott-Price, V., Hernandez, D.G., Nalls, M.A., Clark, L.N., Honig, L.S., et al. (2014). Genetic analysis implicates APOE, SNCA and suggests lysosomal dysfunction in the etiology of dementia with Lewy bodies. *Hum. Mol. Genet.* *23*, 6139–6146.
25. Tagliaferro, L., and Chiba-Falek, O. (2016). Up-regulation of SNCA gene expression: implications to synucleinopathies. *Neurogenetics* *17*, 145–157.
26. Chiba-Falek, O., Lopez, G.J., and Nussbaum, R.L. (2006). Levels of alpha-synuclein mRNA in sporadic Parkinson disease patients. *Mov. Disord.* *21*, 1703–1708.
27. Linnertz, C., Lutz, M.W., Ervin, J.F., Allen, J., Miller, N.R., Welsh-Bohmer, K.A., Roses, A.D., and Chiba-Falek, O. (2014). The genetic contributions of SNCA and LRRK2 genes to Lewy Body pathology in Alzheimer's disease. *Hum. Mol. Genet.* *23*, 4814–4821.
28. Lutz, M.W., Saul, R., Linnertz, C., Glenn, O.C., Roses, A.D., and Chiba-Falek, O. (2015). A cytosine-thymine (CT)-rich haplotype in intron 4 of SNCA confers risk for Lewy body pathology in Alzheimer's disease and affects SNCA expression. *Alzheimers Dement.* *11*, 1133–1143.
29. Gründemann, J., Schlaudraff, F., Haecel, O., and Liss, B. (2008). Elevated alpha-synuclein mRNA levels in individual UV-laser-microdissected dopaminergic substantia nigra neurons in idiopathic Parkinson's disease. *Nucleic Acids Res.* *36*, e38.
30. Rockenstein, E., Hansen, L.A., Mallory, M., Trojanowski, J.Q., Galasko, D., and Masliah, E. (2001). Altered expression of the synuclein family mRNA in Lewy body and Alzheimer's disease. *Brain Res.* *914*, 48–56.
31. McCormack, A.L., Mak, S.K., Henderson, J.M., Bumcrot, D., Farrer, M.J., and Di Monte, D.A. (2010). Alpha-synuclein suppression by targeted small interfering RNA in the primate substantia nigra. *PLoS One* *5*, e12122.
32. Takahashi, M., Suzuki, M., Fukuoka, M., Fujikake, N., Watanabe, S., Murata, M., Wada, K., Nagai, Y., and Hohjoh, H. (2015). Normalization of Overexpressed alpha-Synuclein Causing Parkinson's Disease By a Moderate Gene Silencing With RNA Interference. *Mol. Ther. Nucleic Acids* *4*, e241.
33. Flierl, A., Oliveira, L.M.A., Falomir-Lockhart, L.J., Mak, S.K., Hesley, J., Soldner, F., Arndt-Jovin, D.J., Jaenisch, R., Langston, J.W., Jovin, T.M., and Schüle, B. (2014). Higher vulnerability and stress sensitivity of neuronal precursor cells carrying an alpha-synuclein gene triplication. *PLoS One* *9*, e112413.
34. Guhathakurta, S., Bok, E., Evangelista, B.A., and Kim, Y.S. (2017). Deregulation of alpha-synuclein in Parkinson's disease: Insight from epigenetic structure and transcriptional regulation of SNCA. *Prog. Neurobiol.* *154*, 21–36.
35. Jowaed, A., Schmitt, I., Kaut, O., and Wüllner, U. (2010). Methylation regulates alpha-synuclein expression and is decreased in Parkinson's disease patients' brains. *J. Neurosci.* *30*, 6355–6359.
36. Wang, Y., Wang, X., Li, R., Yang, Z.F., Wang, Y.Z., Gong, X.L., and Wang, X.M. (2013). A DNA methyltransferase inhibitor, 5-aza-2'-deoxycytidine, exacerbates neurotoxicity and upregulates Parkinson's disease-related genes in dopaminergic neurons. *CNS Neurosci. Ther.* *19*, 183–190.
37. Matsumoto, L., Takuma, H., Tamaoka, A., Kurisaki, H., Date, H., Tsuji, S., and Iwata, A. (2010). CpG demethylation enhances alpha-synuclein expression and affects the pathogenesis of Parkinson's disease. *PLoS One* *5*, e15522.
38. Gu, J., Barrera, J., Yun, Y., Murphy, S.K., Beach, T.G., Woltjer, R.L., Serrano, G.E., Kantor, B., and Chiba-Falek, O. (2021). Cell-Type Specific Changes in DNA Methylation of SNCA Intron 1 in Synucleinopathy Brains. *Front. Neurosci.* *15*, 652226.
39. Kantor, B., Tagliaferro, L., Gu, J., Zamora, M.E., Ilich, E., Grenier, C., Huang, Z.Y., Murphy, S., and Chiba-Falek, O. (2018). Downregulation of SNCA Expression by Targeted Editing of DNA Methylation: A Potential Strategy for Precision Therapy in PD. *Mol. Ther.* *26*, 2638–2649.
40. Tagliaferro, L., Ilich, E., Moncalvo, M., Gu, J., Sriskanda, A., Grenier, C., Murphy, S.K., Chiba-Falek, O., and Kantor, B. (2019). Lentiviral Vector Platform for the Efficient Delivery of Epigenome-editing Tools into Human Induced Pluripotent Stem Cell-derived Disease Models. *J. Vis. Exp.* *145*.
41. Yeo, N.C., Chavez, A., Lance-Byrne, A., Chan, Y., Menn, D., Milanova, D., Kuo, C.C., Guo, X., Sharma, S., Tung, A., et al. (2018). An enhanced CRISPR repressor for targeted mammalian gene regulation. *Nat. Methods* *15*, 611–616.
42. Singleton, A.B., Farrer, M., Johnson, J., Singleton, A., Hague, S., Kachergus, J., Hulihan, M., Peuralinna, T., Dutra, A., Nussbaum, R., et al. (2003). alpha-Synuclein locus triplication causes Parkinson's disease. *Science* *302*, 841.
43. Waters, C.H., and Miller, C.A. (1994). Autosomal dominant Lewy body parkinsonism in a four-generation family. *Ann. Neurol.* *35*, 59–64.
44. Byers, B., Cord, B., Nguyen, H.N., Schüle, B., Fenno, L., Lee, P.C., Deisseroth, K., Langston, J.W., Pera, R.R., and Palmer, T.D. (2011). SNCA triplication Parkinson's patient's iPSC-derived DA neurons accumulate alpha-synuclein and are susceptible to oxidative stress. *PLoS One* *6*, e26159.
45. Liu, H., and Zhang, S.C. (2011). Specification of neuronal and glial subtypes from human pluripotent stem cells. *Cell. Mol. Life Sci.* *68*, 3995–4008.
46. Lee, M.K., Tuttle, J.B., Rebhun, L.I., Cleveland, D.W., and Frankfurter, A. (1990). The expression and posttranslational modification of a neuron-specific beta-tubulin iso-type during chick embryogenesis. *Cell Motil Cytoskeleton* *17*, 118–132.
47. Lee, V.M., and Pixley, S.K. (1994). Age and differentiation-related differences in neuron-specific tubulin immunostaining of olfactory sensory neurons. *Brain Res. Dev. Brain Res.* *83*, 209–215.
48. Menezes, J.R., and Luskin, M.B. (1994). Expression of neuron-specific tubulin defines a novel population of the proliferative layers of the developing telencephalon. *J. Neurosci.* *14*, 5399–5416.
49. Gilyarov, A.V. (2008). Nestin in central nervous system cells. *Neurosci. Behav. Physiol.* *38*, 165–169.
50. Lendahl, U., Zimmerman, L.B., and McKay, R.D. (1990). CNS stem cells express a new class of intermediate filament protein. *Cell* *60*, 585–595.
51. Haavik, J., and Toska, K. (1998). Tyrosine hydroxylase and Parkinson's disease. *Mol. Neurobiol.* *16*, 285–309.
52. Oda, Y. (1999). Choline acetyltransferase: the structure, distribution and pathologic changes in the central nervous system. *Pathol. Int.* *49*, 921–937.
53. Tagliaferro, L., Zamora, M.E., and Chiba-Falek, O. (2019). Multiplication of the SNCA locus exacerbates neuronal nuclear aging. *Hum. Mol. Genet.* *28*, 407–421.
54. Tagliaferro, L., Glenn, O.C., Zamora, M.E., Beach, T.G., Woltjer, R.L., Lutz, M.W., and Chiba-Falek, O. (2017). Genetic analysis of alpha-synuclein 3' untranslated region and its corresponding microRNAs in relation to Parkinson's disease compared to dementia with Lewy bodies. *Alzheimers Dement.* *13*, 1237–1250.
55. Kantor, B., Odonovan, B., Rittiner, J., Lindner, N., Dong, W., Zhang, A., Nicholls, P., and Chiba-Falek, O. (2023). All-in-one AAV-delivered epigenome-editing platform: proof-of-concept and therapeutic implications for neurodegenerative disorders. Preprint at bioRxiv. <https://doi.org/10.1101/2023.04.14.536951>.
56. Anderson, J.P., Walker, D.E., Goldstein, J.M., de Laat, R., Banducci, K., Caccavello, R.J., Barbour, R., Huang, J., Kling, K., Lee, M., et al. (2006). Phosphorylation of Ser-129 is the dominant pathological modification of alpha-synuclein in familial and sporadic Lewy body disease. *J. Biol. Chem.* *281*, 29739–29752.
57. Fujiwara, H., Hasegawa, M., Dohmae, N., Kawashima, A., Masliah, E., Goldberg, M.S., Shen, J., Takio, K., and Iwatsubo, T. (2002). alpha-Synuclein is phosphorylated in synucleinopathy lesions. *Nat. Cell Biol.* *4*, 160–164.
58. Thorne, N.J., and Tumbarello, D.A. (2022). The relationship of alpha-synuclein to mitochondrial dynamics and quality control. *Front. Mol. Neurosci.* *15*, 947191.
59. Ran, F.A., Cong, L., Yan, W.X., Scott, D.A., Gootenberg, J.S., Kriz, A.J., Zetsche, B., Shalem, O., Wu, X., Makarova, K.S., et al. (2015). In vivo genome editing using Staphylococcus aureus Cas9. *Nature* *520*, 186–191.
60. MacDougall, G., Brown, L.Y., Kantor, B., and Chiba-Falek, O. (2021). The Path to Progress Preclinical Studies of Age-Related Neurodegenerative Diseases: A Perspective on Rodent and hiPSC-Derived Models. *Mol. Ther.* *29*, 949–972.
61. Park, J.C., Jang, S.Y., Lee, D., Lee, J., Kang, U., Chang, H., Kim, H.J., Han, S.H., Seo, J., Choi, M., et al. (2021). A logical network-based drug-screening platform for Alzheimer's disease representing pathological features of human brain organoids. *Nat. Commun.* *12*, 280.
62. Gorbatyuk, O.S., Li, S., Nash, K., Gorbatyuk, M., Lewin, A.S., Sullivan, L.F., Mandel, R.J., Chen, W., Meyers, C., Manfredsson, F.P., and Muzyczka, N. (2010). In vivo RNAi-mediated alpha-synuclein silencing induces nigrostriatal degeneration. *Mol. Ther.* *18*, 1450–1457.

63. Khodr, C.E., Sapru, M.K., Pedapati, J., Han, Y., West, N.C., Kells, A.P., Bankiewicz, K.S., and Bohn, M.C. (2011). An alpha-synuclein AAV gene silencing vector ameliorates a behavioral deficit in a rat model of Parkinson's disease, but displays toxicity in dopamine neurons. *Brain Res.* *1395*, 94–107.
64. Vijayraghavan, S., and Kantor, B. (2017). A Protocol for the Production of Integrase-deficient Lentiviral Vectors for CRISPR/Cas9-mediated Gene Knockout in Dividing Cells. *J. Vis. Exp.* *130*, 56915.
65. Lin, L., Göke, J., Cukuroglu, E., Dranias, M.R., VanDongen, A.M.J., and Stanton, L.W. (2016). Molecular Features Underlying Neurodegeneration Identified through In Vitro Modeling of Genetically Diverse Parkinson's Disease Patients. *Cell Rep.* *15*, 2411–2426.
66. Crompton, L.A., Byrne, M.L., Taylor, H., Kerrigan, T.L., Bru-Mercier, G., Badger, J.L., Barbuti, P.A., Jo, J., Tyler, S.J., Allen, S.J., et al. (2013). Stepwise, non-adherent differentiation of human pluripotent stem cells to generate basal forebrain cholinergic neurons via hedgehog signaling. *Stem Cell Res.* *11*, 1206–1221.
67. Tabassam, Q., Ahmed, S., Mehmood, T., Iqbal, M., Saeed, S., Ahmad, M.M., Sultan, A., Rehman, M.M.U., Qadir, R., Ullah, A., and Abdul Rehman, N. (2021). Phytochemical investigation and effective therapeutic potential of plants extracts against breast and ovarian cancer cell lines: compounds from *Zizyphus mauritiana* and *triticum aestivum*. *Cell. Mol. Biol.* *67*, 147–152.
68. Haidar, S., Aichele, D., Birus, R., Hielscher, J., Laitinen, T., Poso, A., and Jose, J. (2019). In Vitro and in Silico Evaluation of Bikaverin as a Potent Inhibitor of Human Protein Kinase CK2. *Molecules* *24*, 1380.
69. Basti, A., Malhan, D., Dumbani, M., Dahlmann, M., Stein, U., and Relógio, A. (2022). Core-Clock Genes Regulate Proliferation and Invasion via a Reciprocal Interplay with MACC1 in Colorectal Cancer Cells. *Cancers* *14*, 3458.